

Chemical analysis of carbonaceous particles inside Cu wire molten by electrical arcing

Byung-wook Ahn^{a,1}, Jungyong Kim^{b,1}, Seungsu Kang^a, Suar Oh^a, Giheon Kim^a,
Woo-Sung Jang^a, Eunju Yeo^c, Young-Min Kim^a, Young Chul Choi^{d,*}, Dong-soon Kwag^{c,**},
Seong Chu Lim^{a,e,***}

^a Department of Energy Science, Sungkyunkwan University (SKKU), Suwon, 16419, Republic of Korea

^b CFEL Co., Ltd., Hongcheon-gun, 25115, Gangwon-do, Republic of Korea

^c Department of Fire Safety, Kyungil University, Gyeongsan-si, Gyeongsangbuk-do, 38428, Republic of Korea

^d Korea Carbon Industry Promotion Agency, Jeonju-si, Jeollabuk-do, 54853, Republic of Korea

^e Department of Smart Fab. Technology, Sungkyunkwan University (SKKU), Suwon 16419, Republic of Korea

ARTICLE INFO

Keywords:

Carbonaceous nanostructures
Chemical bonding
Electric arcing
Cause of the fire

ABSTRACT

We characterized carbonaceous nanostructures, which were produced from the electrical arcing of the current-carrying Cu wires. The nanostructures are prepared in two different ways. The electrical arc is provoked by partially removing the polyvinyl chloride (PVC) insulation. In this case, PVC is exposed to electrical arcing, and it becomes the carbon structure after the arcing. In the other case, the insulation is intentionally burned, and the current-carrying Cu wire is left until they were electrically short. Thus, the carbonized PVC is exposed to electrical arcing. Our analysis of these two different carbon materials reveals that the chemical binding of carbon, the elements, the diffusion of carbon into Cu wire, and the relative distribution of the carbon are quite dissimilar. The distinctions between the carbon soot resulting from different arcing conditions can be used to decipher the cause of the fire, which has remained unsolved to date.

1. Introduction

Carbon is one of the most common elements, including oxygen, hydrogen, and nitrogen. Among them, in particular, carbon exists in many different atomic structures, i.e., 0D fullerene, 1D carbon nanotube, 2D graphene, and 3D diamond [1]. The carbon allotropes retrieve not only different atomic structures but also distinct electronic features. For instance, the diamond, a pyramidal structure, is an electrical insulator with a bandgap of 5.47 eV [2], whereas graphene, a 2D carbon sheet, is a semimetal with zero energy gap [3]. In the case of carbon nanotubes, both semiconductor and metal are found. Furthermore, their electronic structures are highly subject to the diameter and the chiral angles [4,5]. All these carbon allotropes can be synthesized using CH₄ and C₂H₂ by employing different catalytic metals. However, they display very different material properties [6–8].

Similar to crystalline carbon materials, carbonaceous materials, which are composed of *sp*, *sp*², and *sp*³ hybridized, are amorphous, and their mechanical and electrical properties widely vary depending on the composition ratio [9]. The formation of different types of *sp* bond has been controlled via the precursor and growth conditions, including temperature, pressure, gas species, and catalyst. In the case of diamond-like carbon (DLC), it is an amorphous material that demonstrates physical properties similar to that of the diamond [10]. Therefore, it has a high hardness. Such physical properties enable them as coating layers for abrasive tools. Different from DLC, graphitic carbons contain *sp*² layered structures of the size of a few nm. Its unique structures make it useful for Li-ion batteries (LIB) for anode materials [11]. The synthesis of graphitic carbon is usually carried out at a temperature above 2000 K. The carbonaceous structure exists in various forms, depending on the synthetic conditions, including temperature, pressure,

* Corresponding author.

** Corresponding author.

*** Corresponding author.

E-mail addresses: youngchoi@kcarbon.or.kr (Y.C. Choi), diskwag@kiu.kr (D.-s. Kwag), seonglim@skku.edu (S.C. Lim).

¹ These authors contributed equally to the work.

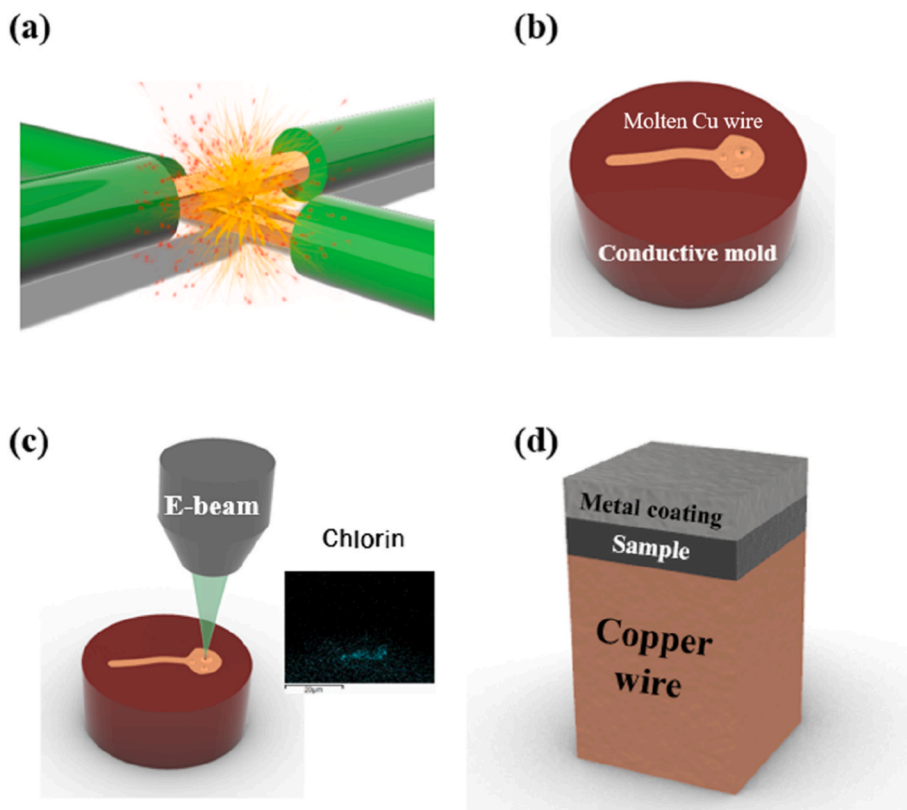


Fig. 1. Schematic of sample preparation. (a) Shorting of electrical wires. (b) Mounting and polishing of molten Cu wire. (c) SEM/EDS characterizations for sampling of carbon structures in molten Cu wire. (d) TEM sample preparation for chemical and elemental analyses on carbon particles. (A colour version of this figure can be viewed online.)

precursor, and ambient gases. This implies that the growth conditions can be retraced if the chemical nature and composition can be analyzed.

In this study, we characterize the carbonaceous particles captured inside Cu wires that were fused because of an electrical arcing. During the arcing, the carbon particles in the vicinity of the arcing were captured in a molten Cu wire. Therefore, by characterizing the carbon microstructure buried inside Cu wire, we probably are able to decipher the cause of the fire, whether it was the result of an electrical arc or not. For instance, if the arcing is the cause of the fire, the carbon

microstructures were produced from the wire insulation that was carbonized by electrical arcing. However, if the arcing is the result of the fire, the microstructures were yielded from carbon soot that was exposed to the arcing. Thus, the carbon structures are expected to be different. Our approach to analyzing the chemical bonding natures of carbon atoms, their distribution, together with elemental mapping of the carbon soot embedded in Cu wire, is expected to provide a new protocol that reveals the cause of the fire at the crime scenes.

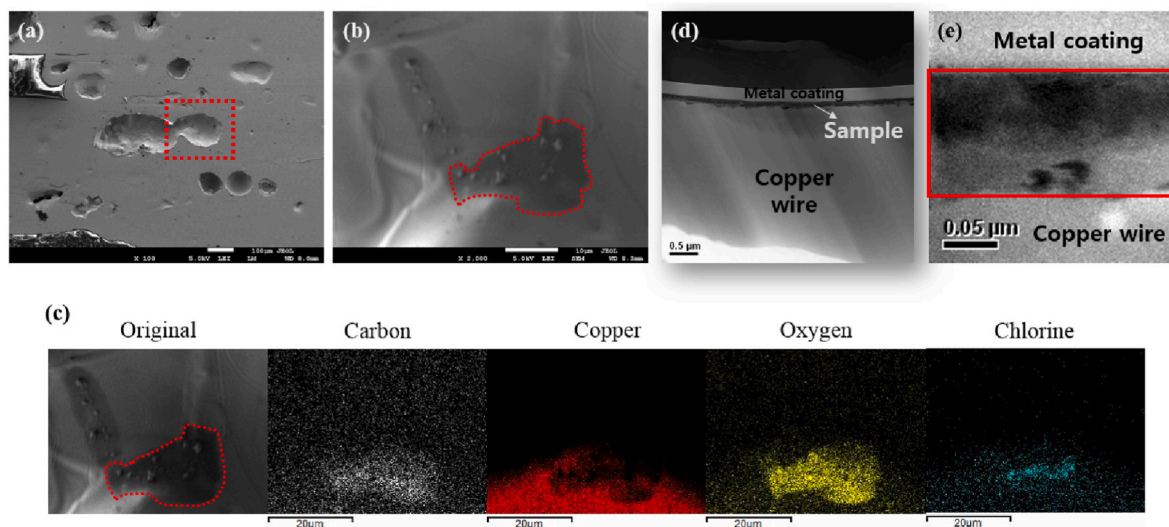


Fig. 2. SEM images of (a) sectioned and polished molten bead, (b) carbon soot inside a bead. (c) Element mapping of carbon soot. (d) Locally laminated Cu bead produced using FIB. (e) Zoomed-in image of the sample in Fig. 2(d). (A colour version of this figure can be viewed online.)

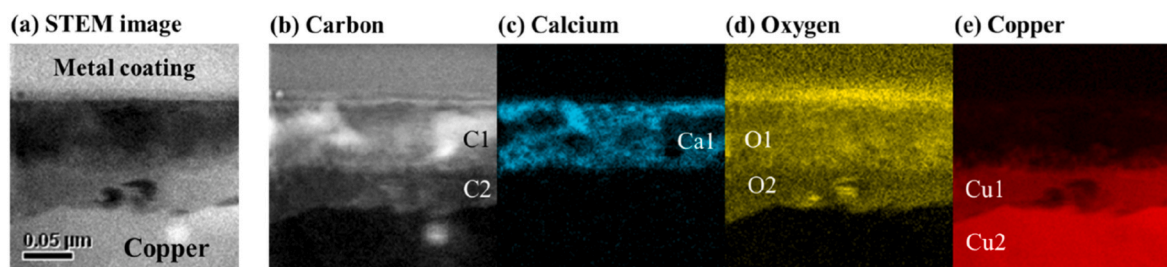


Fig. 3. (a) Cross-sectional image of direct bead. (b)–(e) Element mapping of direct bead. (A colour version of this figure can be viewed online.)

2. Experimental section

We produced carbon particles using electrical arcing. To cause an electrical arcing, we used a sulfuric-acid battery that supplies electrical current at 12 V to Cu wires that are in tight contact [Supplementary Information 1]. For a direct arcing, the insulation of the wire was partially peeled off, as shown in Fig. 1(a), for producing an electrical short, and a molten bead of Cu wire was formed as soon as the battery was switched on. For an indirect arcing, the current-carrying wires were set on fire, using a gas torch. Then, they were left burning until the electrical arcing occurred between them. In both cases, after the electrical breakdown, the fire was extinguished immediately. Therefore, no effect of the residual fire appeared in our investigations. We collected the molten Cu balls and cleaned them in acetone solution using a sonicator to remove the impurities on the surface. The investigation on the carbon particles was conducted by following the procedures shown in Fig. 1. First, we ground and polished the molten Cu beads to open them, as shown in Fig. 1(b) [Supplementary Information 3]. It is expected that, at the moment of arcing, the wire melted owing to a surge of electrical power, following which it suddenly solidified. However, within the fragment of a second, during arcing, the ashes from the fire could be captured inside the molten area, which could contain key evidence on the cause of the fire. Furthermore, this evidence would have been secured from the loss by the residual fire and contamination by the fire extinguisher and other ashes.

The specimen was sectioned in order to search for the carbon nanostructures captured inside Cu bead shown in Figs. S1(d) and S1(h). In this process, scanning electron microscopy (SEM) and energy dispersive x-ray spectroscopy (EDXS) were employed in the search for the debris, as shown in Fig. 1(c). Once carbon particles were found inside the beads, local micromachining using the focused-ion beam (FIB) technique was used to laminate the Cu wire locally and mount it on a transmission electron microscope (TEM) grid for elemental and chemical studies, as shown in Fig. 1(d).

3. Results and discussion

Fig. 2 (a) is an SEM image of the cross-sectioned Cu wire. The figure indicates the presence of several dints, whose formation is accounted for as follows: The wire used in this study was a stranded wire, and not a solid one. Therefore, physical gaps existed, before electrical melting.

During arcing, a significantly large current flowed, and the temperature of the stranded wire increased beyond the melting point of Cu. When the stranded wires coalesced during arcing, the gap filled up; however, some gases and ashes could have been trapped in them. Most of the pits observed in Fig. 2(a) were empty or filled with minute amounts of ashes. When zooming in on one of the pits in Fig. 2(a), a thin layer of carbon was found inside the pit, which is marked by the dashed red line in Fig. 2 (b). In-situ elemental analyses of the thin carbon layer were performed using EDXS to verify whether the carbon layer under study was sourced from the conducting paste or from the PVC insulation. The insulation of an electrical wire is usually prepared by adding Cl, CaCO_3 , and $\text{Al}(\text{OH})_3$ into the polymer insulator in order to retard the fire fumes [Supplementary Information 2]. However, such elements were not present inside the conducting paste used for mechanical polishing [Supplementary Information 3]. Once the origin of the carbon ash was confirmed, we collected the sample for elaborate chemical analyses, which were conducted using TEM.

Fig. 2(d) is an SEM image of the sample prepared using the FIB technique. Our carbon sample was protected with a W coating during the FIB process. The carbon layer in the figure was sandwiched between the metal coating and Cu wire. The thickness of the sample in Fig. 2(e) is approximately 100–150 nm. Further probing of the chemical status and concentration of the tiny carbon material was performed using scanning TEM (STEM).

Figs. 3 and 4 are results of electron microscopies and spectroscopies of both tiny Cu beads obtained from direct (referred to as direct bead) and indirect arcing (referred to as indirect bead). Fig. 3(a) is an image acquired from a direct bead. From the bead, four major different elements, C, Ca, O, and Cu were detected as demonstrated in Fig. 3(b–e). In the case of Al, the occurrence is not consistent from EDXS. To control the flame-retardant properties of electrical wire, the composition ratio of each additive varies, including burning speed, smoke density, and oxygen index. Therefore, we consider that the weighing ratio of $\text{Al}(\text{OH})_3$ is not as high as other retarding additives. In the sample, element mapping was carried out using electron energy-loss spectroscopy (EELS, JEM-2100F/CESCCR, JEOL, see Supplementary Information 4 for details). First, from the carbon mapping in Fig. 3(b), a strong EELS signal was found at the surface marked as C1, which expands down to ~100 nm from the surface in Fig. 3(b). The intensity weakened in the area further below, marked as C2. In addition to carbon, Ca was also detected, which could have been added into the PVC coating, in the form of CaCO_3 , an

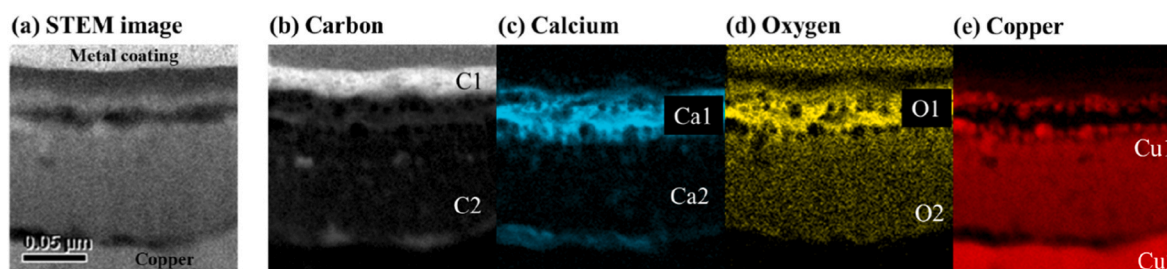


Fig. 4. (a) Cross-sectional image of the indirect bead. (b)–(e) Element mapping of the indirect bead. (A colour version of this figure can be viewed online.)

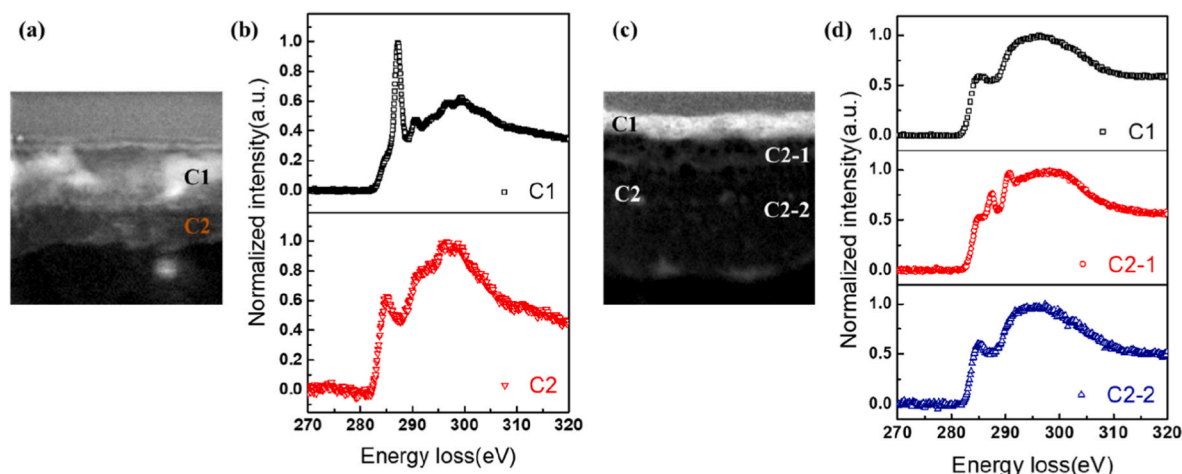


Fig. 5. (a) Local TEM image and (b) carbon electron energy-loss (EEL) spectra of the direct bead. (c) Local TEM image and (d) carbon EELS spectra of the indirect bead. (A colour version of this figure can be viewed online.)

incombustible ingredient. Ca was also found with high intensity in the Ca1 region. Unlike the case of C, an intensity gradient was not observed for Ca. Considering the fact that Ca1 matched C1, the carbon from the C1 area could be expected to have been sourced from CaCO_3 , further supporting the fact that the carbon ash resulted from the PVC coating of the wire burnt by the electrical arc. Thus, the existence of Ca drew a line for the Cu surface; the Cu wire existed right below Ca. The EELS mapping of Ca implied that the carbon in the C2 region could have diffused into the Cu wire, producing a different chemical nature. This assumption was further validated when the carbon EELS was compared to that of Cu. As shown in Fig. 3(e), the EELS of Cu exhibits an intensity gradation. The signal from the Cu1 region was weaker than that from the Cu2 region. It is interesting that Cu1 matched C2, indicating that the weak EELS signal in the Cu1 region was due to the infiltration of carbon into the Cu wire at the surface. No carbon signal was detected below Cu1.

The difference in the oxygen concentration on a direct bead was not clear because it was abundant not only in air but also on the surface of Cu. However, it is intriguing to note that the penetration depth of oxygen was coincident with that of carbon. Therefore, the existence of copper oxide could be anticipated in the Cu1 region. In this area, the observed oxygen could be attributed to the natural CuO_x . However, the coincidence of the Cu1 layer with the C2 layer supported the possibility that Cu1 was related to the bead formation. As evidence, only Cu was detected in Cu2, and the boundary between Cu1 and Cu2 was abrupt.

Fig. 4(a) shows an image of the indirect bead. The elemental mapping obtained via EELS appears to be quite different from that of the direct bead shown in Fig. 3(a). The most noticeable differences between the direct and indirect beads were in the depth profiles of the four major elements. Much deeper diffusion was observed in the indirect bead than in the direct bead. Their overall depth profiles extended over 130 nm, as shown in Fig. 3(a). A strong but thin carbon layer was formed on the surface marked by C1, approximately 20 nm in depth. Below this, a faded and weak carbon signal (C2 region) stretched down to 200 nm from C1. Between the Ca1 and Ca2 regions, the signal from Ca showed a strong contrast in intensity. Such gradation in EELS from Ca did not exist in the case of the direct bead. Therefore, it is believed that Ca1 from the PVC coating mostly inhabited the Ca1 area. Because of the high wire temperature of the indirect case, Ca diffused much further into the Cu wire (region Ca2) than Ca in the direct case. In the case of the indirect bead, the boundary between Cu wire and carbon ash was not clearly distinguishable. As can be noticed from the direct bead, the smearing of C and Ca into the wire directly affected the local EELS signal of Cu. In Fig. 4(e), the EELS signal of Cu is quite inhomogeneous, with strong intensity contrast. We zoned the Cu wire as Cu1 and Cu2 depending on the contamination of other elements. Inside the Cu1 region, oxygen, Ca,

and carbon intermixed, whereas only the Cu signal was detected in Cu2. A comparison between Figs. 3 and 4 indicated that the most prominent difference was in the overall distribution of Ca. When the wire was hot, diffusion of Ca was feasible in the Cu wire.

In addition to the elemental mapping, EELS allows us to understand the chemical binding nature. The chemical characteristics of carbon were studied as functions of the depth, using which we expected to find more crucial evidence distinguishing the formation of direct and indirect arcing. Between the direct and indirect ones, the carbon display was quite different in the EEL spectra, as shown in Fig. 5(b). For instance, inside the C1 region, a sharp and strong peak at approximately 287 eV, corresponding to hydroxyl or epoxide groups [12], dominated other peaks. A lower energy peak at 285 eV was weak, which could be attributed to the sp^2 carbons [12–16]. In addition, a peak at ~ 290 eV, known for carbonate ions CO_3^{2-} [17–19], characterized the carbon from the CaCO_3 layer. The EEL spectra of C2 were quite different from the ones of C1. The peak from the hydroxyl or epoxide groups was not found. Instead, the sp^2 carbon peak at 285 eV was stronger than that in the case of C1. The fact that the peak from carbonate ions at ~ 290 eV was not noticeable agrees with the absence of CaCO_3 in region 2. As the carbon K edge fine structure from EELS in Fig. 5(a) is subject to change, depending on the oxidation level and chemical composition, different EEL spectra could be anticipated for C1 and C2. Together with the elemental analysis, EELS studies provide another method to ascertain the cause of the fire.

The EEL spectra from the indirect bead were obtained and are compared in Fig. 5(d). In addition, the sample morphology is provided in Fig. 5(c). The top layer, C1, showing a strong C peak in Fig. 4(b), revealed two peaks at 285 and 296 eV. Among them, the peak at 296 eV was very broad and featureless in EELS. Such a peak shape signified amorphous carbon materials inside which sp^2 and sp^3 carbons were mixed together [20,21]. In the C2 region, which showed a significant homogenous C concentration, EELS were obtained at two different locations, C2-1 and C2-2. At C2-1, small peaks were observed within the energy range between 285 and 296 eV, which expectedly originated from CaCO_3 . Among these, the peak at 287 eV could be attributed to the hydroxyl or epoxide groups [12] and that at 290 eV could be attributed to the carbonate ions. The observation of the peaks at 287 and 290 eV were in agreement with the results in region 1 of the direct bead. Therefore, it could be expected that CaCO_3 was strongly localized in C2-1 region, which meant that CaCO_3 most probably existed on the surface of the Cu wire.

It is interesting to note that, below C2-1, amorphous features were observed again in C2-2. The comparison of EELS between Fig. 5(b) and (d) indicated that the carbon species inside CaCO_3 and the Cu wire has

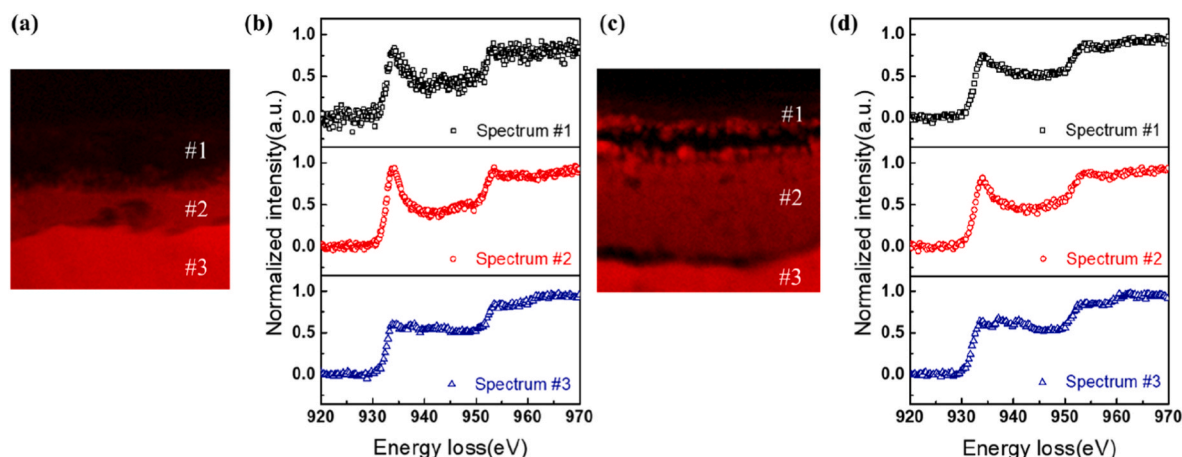


Fig. 6. (a) Cu element map and (b) EELS of the direct bead. (c) Cu element map and (d) EELS of the indirect bead. (A colour version of this figure can be viewed online.)

different chemical natures, as shown in the figures. This could probably be due to the different carbonization levels of the PVC insulator at the moment of the electrical spark. In the case of the direct bead, the wire was cold and no carbonization occurred in the insulator. However, in the indirect case, the wire was hot and the insulator was already burnt. Amorphous carbon was formed before the arcing. The two different carbon materials were introduced into the Cu wire at different depths, as shown in Fig. 5(a) and (c).

The chemical properties of the Cu wire, depending on the location, were characterized as shown in Fig. 6. The spectral intensity of Cu EEL became stronger as the depth increased, in both direct and indirect beads. The intensity of EELS changed depending on the infiltration of Ca, C, and O. Thus, with respect to the elements inside the Cu wire, the chemical nature of Cu could be expected to be depth-dependent. For this reason, we zoned Cu into three different regions for both the direct bead in Fig. 5(a) and indirect bead in Fig. 5(b). Pure Cu possesses two edge peaks at 933–935 eV (L_3) and 952–954 eV (L_2) [22,23]. The EEL spectra in region 3 from both direct and indirect beads clearly manifested these edge peaks in Fig. 6(a) and (c). Therefore, it is reasonable to say that region 3 was occupied by pure Cu. However, as we moved into regions 1 and 2, the Cu wire was infiltrated by C, O, and Ca elements. As a result, both the edge peaks, L_2 and L_3 from regions 1 and 2, became sharper than the ones in region 3. However, with respect to 931 eV (L_3) in region 3, the shift was not noticeable. For copper oxides, the positions of the two edge peaks typically shift slightly, by less than 1 eV, compared to pure Cu, which is coincident with the results shown in Fig. 5(a) and (b). Instead, the edge peaks became more prominent when the oxygen content increased inside Cu. Thus, the peak intensities of L_3 and L_2 became more prominent with the formation of CuO, rather than Cu_2O . The result indicated that, in the case of Cu, the formation of Cu_2O was more dominant, when compared to that of CuO. It is yet unclear why a different form of copper oxide, CuO, is not yielded. Our EELS analysis on Cu implies that the oxidation states of Cu itself may not be able to provide any traits that are informative enough to distinguish between the direct and indirect beads, as only one chemical state is present.

4. Conclusions

Elemental and chemical analyses of the carbonaceous nanostructures produced at the moment of electrical spark were performed. As carbonous particles were enclosed by molten Cu wire, they were secure from contamination. The analysis supported that the direct and indirect arcing resulted in the formation of carbon dusts that had different elemental distributions and chemical natures. In particular, the chemical bond of carbon materials was distinctive, between direct and indirect

arcing, whereas, the chemical states of Cu, observed as Cu_2O , were identical regardless of the cause of the spark. Our results implied that the ingredients and their binding natures inside carbonaceous particles could be used to discover the cause of fire at the site. Nevertheless, to obtain consensus on this method, many different case studies need to be carried out. Although the fire begins by the same cause, it can be put out by different ways. And then, the carbon product can present quite dissimilar chemical and elemental characteristics.

CRediT authorship contribution statement

Byung-wook Ahn: Investigation, Visualization, Writing – original draft. **Jungyong Kim:** Investigation, Validation. **Seungsu Kang:** Investigation. **Suar Oh:** Investigation. **Giheon Kim:** Investigation. **Woo-Sung Jang:** Investigation. **Eunju Yeo:** Investigation. **Young-Min Kim:** Investigation. **Young Chul Choi:** Conceptualization, Validation, Writing – original draft, Writing – review & editing. **Dong-soon Kwag:** Conceptualization, Validation, Project administration. **Seong Chu Lim:** Conceptualization, Supervision, Writing – original draft, Writing – review & editing.

Declaration of competing interest

The authors declare that they have no known competing financial interests or personal relationships that could have appeared to influence the work reported in this paper.

Acknowledgements

The authors from SKKU are grateful for the financial support from the ministry of trade, industry and energy (MOTIE) in South Korea under both grant numbers of 20013422 and 20013090.

Appendix A. Supplementary data

Supplementary data to this article can be found online at <https://doi.org/10.1016/j.carbon.2022.12.046>.

References

- [1] S. Nasir, M.Z. Hussein, Z. Zainal, N.A. Yusof, Carbon-based nanomaterials/allotropes: a glimpse of their synthesis, properties and some applications, *Materials* 11 (2018) 295.
- [2] C.J.H. Wort, R.S. Balmer, Diamond as an electrical material, *Mater. Today* 11 (2008) 22–28.
- [3] Y. Zhang, Y.W. Tan, H.L. Stormer, P. Kim, Experimental observation of the quantum Hall effect and berry's phase in graphene, *Nature* 438 (2005) 201–204.

- [4] T.W. Odom, J.-L. Huang, P. Kim, C.M. Lieber, Structure and electronic properties of carbon nanotubes, *J. Phys. Chem. B* 104 (2000) 2794–2809.
- [5] Y.-K. Kwon, D. Tomanek, Electronic and structural properties of multiwall carbon nanotubes, *Phys. Rev. B* 58 (1998), R16001.
- [6] A.M. Cassell, J.A. Raymakers, J. Kong, H. Dai, Large scale CVD synthesis of single-walled carbon nanotubes, *J. Phys. Chem. B* 103 (1999) 6484–6492.
- [7] Y. Shen, A.C. Lua, A facile method for the large-scale continuous synthesis of graphene sheets using a novel catalyst, *Sci. Rep.* 3 (2013) 3037.
- [8] C.J. Lee, S.C. Lyu, H.-W. Kim, J.H. Lee, K.I. Cho, Synthesis of bamboo-shaped carbon–nitrogen nanotubes using $C_2H_2-NH_3-Fe(CO)_5$ system, *Chem. Phys. Lett.* 359 (2002) 115–120.
- [9] H. Sheng, W. Xiong, S. Zheng, C. Chen, S. He, Q. Cheng, Evaluation of the sp^3/sp^2 ratio of DLC films by RF-PECVD and its quantitative relationship with optical band gap, *Carbon Lett.* 31 (2021) 929–939.
- [10] N. Ohtake, M. Hiratsuka, K. Kanda, H. Akasaka, M. Tsujioka, K. Hirakuri, et al., Properties and classification of diamond-like carbon films, *Materials* 14 (2021) 315.
- [11] Q. Cheng, Y. Okamoto, N. Tamura, M. Tsuji, S. Maruyama, Y. Matsuo, Graphene-like-graphite as fast chargeable and high-capacity anode materials for lithium ion batteries, *Sci. Rep.* 7 (2017), 14782.
- [12] A. Tararan, A. Zobelli, A.M. Benito, W.K. Maser, O. Stéphan, Revisiting graphene oxide chemistry via spatially-resolved electron energy loss spectroscopy, *Chem. Mater.* 28 (11) (2016) 3741–3748.
- [13] A. El-Barbary, S. Trasobares, C. Ewels, O. Stephan, A. Okotrub, L. Bulusheva, et al., Electron spectroscopy of carbon materials: experiment and theory, *J. Phys. Conf.* (2006) 149. IOP Publishing.
- [14] D. D'Angelo, C. Bongiorno, M. Amato, I. Deretzis, A. La Magna, E. Fazio, et al., Oxygen functionalities evolution in thermally treated graphene oxide featured by EELS and DFT calculations, *J. Phys. Chem. C* 121 (9) (2017) 5408–5414.
- [15] D. D'Angelo, C. Bongiorno, M. Amato, I. Deretzis, A. La Magna, G. Compagnini, et al., Electron energy-loss spectra of graphene oxide for the determination of oxygen functionalities, *Carbon* 93 (2015) 1034–1041.
- [16] J. Rani, J. Lim, J. Oh, J.-W. Kim, H.S. Shin, J.H. Kim, et al., Epoxy to carbonyl group conversion in graphene oxide thin films: effect on structural and luminescent characteristics, *J. Phys. Chem. C* 116 (35) (2012) 19010–19017.
- [17] J.-W. Kim, T. Kogure, K. Yang, S.-T. Kim, Y.-N. Jang, H.-S. Baik, et al., The characterization of $CaCO_3$ in a geothermal environment: a SEM/TEM-EELS study, *Clay Clay Miner.* 60 (5) (2012) 484–495.
- [18] F. Hofer, P. Golob, New examples for near-edge fine structures in electron energy loss spectroscopy, *Ultramicroscopy* 21 (4) (1987) 379–383.
- [19] L.A. Garvie, A.J. Craven, R. Brydson, Use of electron-energy loss near-edge fine structure in the study of minerals, *Am. Mineral.* 79 (5–6) (1994) 411–425.
- [20] L. Ponnsonnet, C. Donnet, K. Varlot, J. Martin, A. Grill, V. Patel, EELS analysis of hydrogenated diamond-like carbon films, *Thin Solid Films* 319 (1–2) (1998) 97–100.
- [21] F. Langenhorst, V.L. Solozhenko, ATEM-EELS study of new diamond-like phases in the B–C–N system, *Phys. Chem. Chem. Phys.* 4 (20) (2002) 5183–5188.
- [22] J. Ngantcha, M. Gerland, Y. Kihn, A. Rivière, Correlation between microstructure and mechanical spectroscopy of a Cu–Cu₂O alloy between 290 K and 873 K, *Eur. Phys. J. Appl. Phys.* 29 (1) (2005) 83–89.
- [23] W. Chamorro, T. Shyju, P. Boulet, S. Migot, J. Ghanbaja, P. Miska, et al., Role of Cu + on ZnS: Cu p-type semiconductor films grown by sputtering: influence of substitutional Cu in the structural, optical and electronic properties, *RSC Adv.* 6 (49) (2016) 43480–43488.